International Journal of Applied Engineering Research ISSN 0973-4562 Volume 10, Number 17 (2015) pp 38045-38050

Development of Advanced Sonar Sensor Model for Underwater Terrain Mapping based on Occupancy Grids

Sejin Lee
Assistant Professor Division of Mechanical and Automotive Engineering
Kongju National University Cheon an-si, Chung Cheongnam-do, South Korea sejiny3@kongju.ac.kr

Donghyun Kim, Alade O. Tokuta
Assistant Professor, Professor Department of Mathematics and Physics
North Carolina Central University Durham, North Carolina, USA donghyun.kim@nccu.edu, atokuta@nccu.edu

Abstract
This paper presents the advanced sonar sensor model capable of building an underwater terrain map based on the Bayes filter in the manner of the occupancy grid. The proposed sonar sensor model basically considers the losses of received ultrasound intensity according to the underwater absorption and reflection on a terrain surface. The Bayes filter including the advanced sonar sensor model is applied to build an occupancy grid map. The underwater sonar data is acquired by the pencil beam type's sonar sensor mounted on the unmanned surface vehicle (USV). The experimental results show underwater terrain maps before and after applying the proposed method. The depth standard deviations of the terrain grid maps are calculated to evaluate the performance of this approach. With the proposed sonar sensor model, the depth standard deviation average of underwater grid map is decreased by almost 35 percent.

Keywords: Bayes Filter, Occupancy Grid Map, Sonar Sensor Model, Underwater Mapping, USV(Unmanned Surface Vehicle)

Introduction

Unmanned surface vehicles (USV) that perform operations on the surface of the water are robots that are generally used for specific purposes such as environment exploration and monitoring, military reconnaissance, and so on. Recently, the aquatic ecosystems need to be monitored due to rapid changes caused by pollution and environmental damage including the Korean river restoration project. Therefore, a sustainable information system for environmental monitoring and surveillance is required. This has increased the need for low-cost multipurpose USVs that perform underwater terrain monitoring and environment surveillance [1].

Since June 2005, Google has been providing the public with GoogleEarth, a service that provides satellite imagery, maps, terrain information, and 3D building information for the entire globe [2]. This type of data can support various video mapping services for diverse purposes. However, an information system for local underwater terrain such as in specific ponds, dams, and rivers, as well as information on facilities that can be used for agricultural, fishery, and commercial purposes, has not yet been established because of the macroscopic resolution. The three dimensional underwater mapping techniques should be also required to find human bodies and recognize shapes of structures in invisible underwater environments like when the Sewol ferry disaster happened [3].

Even from the disaster prevention and flooding relief perspective, fast underwater search operations are essential during cases of drowning. This is because the analysis of an underwater object's contour can prevent accidents caused by the unplanned entry of a rescue worker and during the process of identifying the location of the drowning person. Therefore, there is a need to develop survey equipment that is easy to use.

Many changes are required as a result of the rapid development of science and technology, as well as the development of information technology in terms of social security and national defense. Furthermore, in an era when the trend of valuing human life is spreading in connection with the development of society and there is a widespread phenomenon of avoiding difficult tasks, it can be said that the development of unmanned systems is one of the best directions to take in strengthening the national defense while responding to the changes in society [4-6].

Research on the three-dimensional mapping of underwater terrain using sensors is an important factor in solving the aforementioned issues, and the most common sensors used underwater are ultrasonic sensors. Jakuba and Yoerger developed an unmanned underwater vehicle called the Autonomous Benthic Explorer (ABE), which mounted the Simrad Mesotech SM2000 ultrasonic sensor, and used it to create the feature maps of the Explorer Ridge and Lost City [7]. Langer and Hebert proposed a method for reconstructing an elevation map of Juan de Fuca Ridge's submarine topography using backscatter images of the ultrasound data [8]. Fairfield's research team introduced a three-dimensional simultaneous localization and mapping (SLAM) technique that uses ultrasonic sensors to navigate a submersible during the exploration of the underwater cave Zacaton Cenote [9]. Williams proposed a method for using ultrasonic sensors to extract the noticeable natural landmarks and then using the collected data to track the position of the submersible [10]. Table 1 lists the major studies on creating ultrasonic sensor-based underwater terrain maps.

This paper proposes a method for building an efficient submarine topographic map using ultrasonic sensors mounted on a USV. In particular, the accuracy and efficiency of the program was achieved though the development of a cartographic technique for creating an occupancy grid map

based on Bayes' theorem, which considers the output loss of the ultrasonic sensors that can occur in an underwater environment. The effectiveness of the underwater terrain mapping model proposed in this study was verified through experiments conducted in an actual lake environment. Section 2 explains the occupancy grid mapping using a Bayes filter. Section 3 explains the characteristics of ultrasonic sensors and the underwater ultrasonic sensors in consideration of the external loss function. Section 4 presents the results of the experiment, and finally, section 5 examines the efficacy of the algorithm based on the results of the experiment.

TABLE.1. Major Studies on Building Ultrasonic Sensor-based Underwater Terrain Maps

Research	Sonar Beam Shape	Map	Resolution / Coverage (m)	Application
[7]	Pencil	Grid	2/2000	Terrain survey
[8]	Wide	Grid	0.25/112	Terrain survey
[9]	Pencil	Grid	0.5/350	SLAM
[10]	Pencil	Point	- /40	Terrain based localization
[11]	Wide	Point	- /200	Terrain based SLAM
[12]	Wide	Point	- /1000	Terrain based SLAM

Occupancy Grid Map

Occupancy grid mapping is one of the methods for the environmental map building using sensor data for an uncertain distance mixed with noise. The environment through which the robot moves is divided into three-dimensional grids, and the terrain map is built by continuously updating the object's occupation probability within each grid using the distance sensor data [13, 14].

A. Grid Map Building

The probability of an occupancy grid map can be expressed as (1):

$$p(m \mid x_{1:t}, z_{1:t}) \tag{1}$$

In (1), m represents the grids that form the map, and consists of N cells, as in m_1, m_2, …, m_i, …, m_N, where m_i, an i-th cell, is the occupational probability of an object. The occupancy status of the grid is presented as a probability value between 0 and 1, and this probability is indicated as $p(m_i)$. In (1), $x_{1:t}$ indicates the location of the robot (USV). The directional angle of the robot, and the x and y coordinates, are used to indicate the location of the robot in this study. The data are calculated as GPS values. $x_{1:t}$ refers to all the robot positions from time step *1* to t, whereas $z_{1:t}$ is all the ultrasonic sensor distance measurements from time step *1* to t. In other words, the occupation probability of the current grid can be calculated through the position of the robot from the start of the operation to its current location, along with its corresponding ultrasound distance measurement.

Generally, a complicated calculation is required to solve (1). Therefore, to simplify the calculation, it was assumed that all the grids were independent of each other. When the occupancy grids are assumed to be independent, (1) can be simplified as follow:

$$p(m \mid x_{1:t}, z_{1:t}) = \prod_{i=1}^{N} p(m_i \mid x_{1:t}, z_{1:t}) \tag{2}$$

B. Occupancy Probability Calculation

Each grid is assumed to be independent of the others, and only the occupancy probability of each cell is calculated. The Bayes filter is applied to (2) in order to represent the equation as a regression equation applicable as an algorithm. A summarization of (2) under the condition of $x_{1:t}$ and $z_{1:t-1}$ is as follow:

$$p(m_i \mid x_{1:t}, z_{1:t}) = p(m_i \mid x_{1:t}, z_{1:t-1}, z_t) \tag{3}$$

In (4), the Bayes filter is applied to the equation above as follow:

$$p(m_i \mid x_{1:t}, z_{1:t-1}, z_t) = \frac{p(z_t \mid m_i, x_t)\, p(m_i \mid x_{1:t}, z_{1:t-1})}{p(z_t \mid x_{1:t}, z_{1:t-1})} \tag{4}$$

In the following equation, the Bayes filter is applied again to the robot's state variables and the probability of the sensor value prediction according to a grid of (4):

$$p(z_t \mid m_i, x_t) = \frac{p(m_i \mid x_t, z_t)\, p(z_t \mid x_t)}{p(m_i \mid x_t)} \tag{5}$$

Here, $p(m_i|x_t)$ is a probability that indicates the occupancy of each grid in accordance with the state of the robot. However, the occupancy of each grid is independent of the robot's state variables because the robot cannot gain any information regarding the environment without receiving sensor values. Therefore, the probability regarding the state of the cell can be expressed as follows:

$$p(m_i \mid x_{1:t}, z_{1:t}) = \frac{p(m_i \mid x_t, z_t)\, p(z_t \mid x_t)}{p(m_i)} \frac{p(m_i \mid x_{1:t-1}, z_{1:t-1})}{p(z_t \mid x_{1:t}, z_{1:t-1})} \tag{6}$$

Using odds will simplify the calculation when creating a regression equation using the Bayes filter, and consequently, the application of the *log odds* ratio produces the following equations:

$$\frac{p(m_i \mid x_{1:t}, z_{1:t})}{p(\bar{m}_i \mid x_{1:t}, z_{1:t})} = \frac{p(m_i \mid x_t, z_t)}{1 - p(m_i \mid x_t, z_t)} \frac{p(m_i \mid x_{1:t-1}, z_{1:t-1})}{1 - p(m_i \mid x_{1:t-1}, z_{1:t-1})} \frac{1 - p(m_i)}{p(m_i)} \tag{7}$$

$$Odds(m_i \mid x_{1:t}, z_{1:t}) = l_t(m_i) = \log \frac{p(m_i \mid x_t, z_t)}{1 - p(m_i \mid x_t, z_t)} + l_{t-1}(m_i) - l_0(m_i) \tag{8}$$

In other words, the *log odds* ratio of the current t step in relation to a grid m_i can be calculated through the *log odds* ratio in relation to m_i at the *t-1* step, the *log odds* ratio in relation to m_i at the initial step, and from the sensor model. The following section explains the underwater ultrasonic sensor model in detail.

Underwater Ultrasonic Sensor Model

A. Definition of Sensor Model

The expression $log(p(m_i|x_t, z_t))/(1-p(m_i|x_t, z_t))$ must be interpreted in order to calculate (8), which was obtained by applying the *log odds* ratio in the previous section. Fig. 1 shows that probability $p(m_i|x_t, z_t)$ can belong to an occupied area or an empty according to the location of cell i depending on the measurement conditions. P_{occ} is used to calculate probability $p(m_i|x_t, z_t)$ when cell i belongs to an occupied area, and P_{emp} is used when it is an empty area. P_{occ} and P_{emp} can be expressed as follows:

$$\begin{cases} p_{occ} = p_{occ}(r_i) \cdot p(\theta_i) \cdot p_{confidence} \\ p_{emp} = p_{emp}(r_i) \cdot p(\theta_i) \cdot p_{confidence} \end{cases} \quad (9)$$

$P_{occ}(r_i)$ in (9) is a probability calculated based on the distance from the location of the sensor to cell i when cell i is within the occupied area, and $P_{emp}(r_i)$ is the probability calculated based on the distance from the location of the sensor to cell i when cell i is within an empty area. $p(\theta_i)$ is the probability calculated based on the angle of cell i to the center of the sensor measurement direction. $p_{confidence}$ is the reliability of the sensor data regarding the measurement conditions.

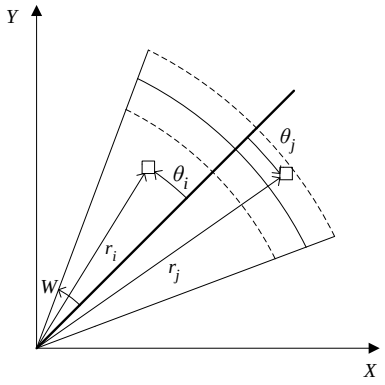

Fig.1. Sensor footprint shape and its variables

B. Occupancy Probability Calculation

The sensor model value in (9) depends on the probabilities with respect to distance r_i, angle θ_i, and $p_{confidence}$. This section explains the probabilities with respect to distance r_i and angle θ_i, and the next section explains $p_{confidence}$.

R in Fig. 2 is the distance from the sensor position to the location of an object recognized by the sensor [15]. The range of $\pm\varepsilon$ from R, which is the distance recognized by the sensor, is recognized as an occupied area, and the range below R-ε (i.e., below R_{min}) is an empty area. The center of the sensor measuring direction with a θ value of 0 in Fig. 3 has a probability of 1, and the probability finally decreases to 0 as the object becomes further away from the center. This equation is expressed as follows:

$$\begin{cases} p_{occ}(r_i) = 1 - \left(\dfrac{r_i - R}{\sqrt{2}\varepsilon}\right)^2 & (R_{min} \le r_i \le R_{max}) \\ p_{emp}(r_i) = \dfrac{r_i^2}{2R_{min}^2} & (0 \le r_i \le R_{min}) \\ p(\theta_i) = 1 - \left(\dfrac{\theta}{W}\right)^2 & (-W \le \theta \le W) \end{cases} \quad (10)$$

Here, W is the value of the angle from the center of the sensor measurement direction to the end of the maximum angle. Therefore, W is the same as the maximum value of θ.

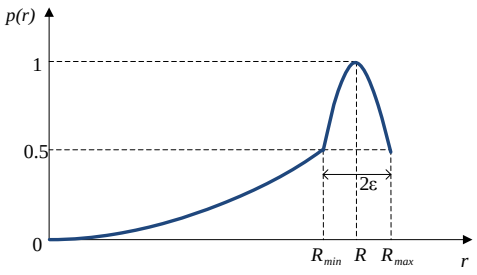

Fig.2. Occupancy probability according to the distance

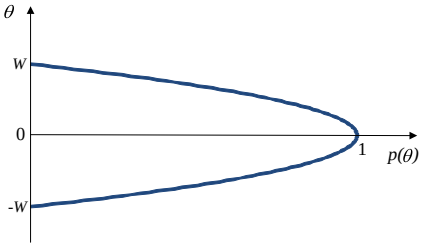

Fig.3. Occupancy probability according to the angle

C. Reliability of Sensor Data

The reliability of the sensor data indicates the reliability of the distance data measured by the sensor in a numerical way. When the intensity of the ultrasound used in the actual measurement is defined as $I_{Evidence}$, and the ideal intensity of the ultrasound theoretically expected is defined as $I_{Acoustic\_Pressure}$, then the reliability of the sensor can be expressed as follows:

$$p_{confidence} = \frac{I_{Evidence}}{I_{Acoustic\_Pressure}} \quad (11)$$

Evidence, the intensity of the ultrasound used in the actual measurement, is the same as the integral values with respect to the measurement intensity by distance shown in Fig. 4. $I_{Evidence}$ is expressed mathematically as shown below:

$$I_{Evidence} = \sum_{i=R-\alpha}^{R+\alpha} ES_i \quad (12)$$

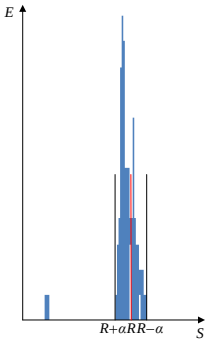

Fig.4. Strength profile of single beam according to the distance

In calculating $I_{Acoustic\_Pressure}$, the ideal theoretical value of the measured intensity, losses such as the loss due to the water absorption (i.e., absorption loss), and collisions with the

underwater terrain (i.e., reflection loss) must be considered. Sections 1 and 3 in Fig. 5 show areas where the intensity of the ultrasound is weakened as a result of water absorption, and this loss is called absorption loss. In contrast, section 2 indicates an ultrasound loss due to collisions with the underwater terrain, and this is called the reflection loss. The directional pressure loss is neglected due to the narrow beam width of a sonar return. This process can be expressed as follows:

$$AcousticPressure = F_{Absorption}(\phi,r) F_{Reflection}(\phi) F_{Absorption}(\phi,r) \quad (13)$$

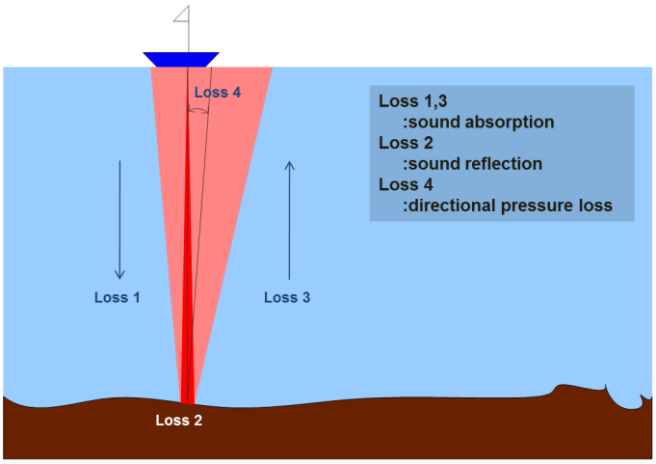

Fig.5. Underwater strength losses of sound waves according to the absorption and reflection

The reflection loss is affected by the material of the reflection surface in collision. Table 2 lists the coefficients of reflection loss by material.

TABLE.2. Reflection Coefficient, C

Material	Impedance, z(Rayles)	C
Air	415	-1
Fresh water	1,480,000	0.04
Salt water	1,540,000	0
Wet fish flesh	1,600,000	0.02
Wet fish bone	2,500,000	0.24
Rubber	1,810,000	0.08
Granite	16,000,000	0.82
Quartz	15,300,000	0.81
Clay	7,700,000	0.67
Sandstone	7,700,000	0.66
Concrete	8,000,000	0.68
Steel	47,000,000	0.94
Brass	40,000,000	0.92
Aluminium	17,000,000	0.83

The resistance loss is divided based on the driving frequency of the ultrasound. A value of 0.6 [dB/m] (approximately 12.9% per meter) is reduced at 1000 kHz (~10 m), and 0.2 [dB/m] (approximately 4.5% per meter) is reduced at 675 kHz (10~100 m) [16]. The reflection loss and resistance loss are expressed as follows:

$$\begin{cases} F_{Absorption}(\phi,r) = \begin{cases} 10^{-0.06r} \times p & at\ 1000kHz \\ 10^{-0.02r} \times p & at\ 675kHz \end{cases} \\ F_{Reflection}(\phi) = C \times p \end{cases} \quad (14)$$

C in $F_{reflection}$ is the loss factor, and can be found in Table 2. A summary of (13) and (14) is as follows:

$$AcousticPressure = \begin{cases} C \times 10^{-0.12r} \times p & at 1000kHz \\ C \times 10^{-0.04r} \times p & at 675kHz \end{cases} \quad (15)$$

A final summary of (11), (12), and (15) for calculating the reliability is as follows:

$$P_{confidence} = \frac{\sum_{i=R-\alpha}^{R+\beta} ES_i}{C \times 10^{-0.01r} \times p} \quad at\ 675kHz \quad (16)$$

Probability $p(m_i|x_t, z_t)$ is obtained through this method to update the sensor model. The following section introduces the experiments and compares the results before and after the application of the sensor model.

Experimental Results

The experiment was conducted at ECHO Park in Los Angeles, CA, USA. An ultrasonic sensor was mounded on the front of a boat, and data regarding the distance and angle from the surface to the underwater terrain along the travel path were collected by manually operating the boat. A comparison of the collected data was conducted before and after applying the Bayes filter, and the excellence of the sensor model proposed in this study was verified.

A. Equipments

The sonar sensor (Imagenex Model 881L) used in this study has a pencil shaped beam with three operating frequencies. The experiment was conducted at 675 kHz. The beam-width at 675 kHz was 1.8°×20°, and the maximum measurable distance was 1000 m. The weight underwater was approximately 0.6 kg, and the price of the equipment was around KRW 10 million (about USD 10,000). Figure 6 and 7 show the sonar sensor of pencil type and USV respectively.

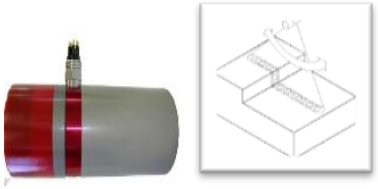

Fig.6. 881L-GS Imaging Sonar Sensor of Imagenex and pencil type beam

Fig.7. Unmanned surface vehicle used in this study

B. Experiments

The experiment was conducted manually as a step size of 2.4° and a scan speed of 0.013 s/degree. The robot including the GPS receiver was driven in a grid pattern as shown in Fig. 8. The experiment was conducted by using an uniform travel path. As shown in Fig. 8, only data from the straight sections were collected during the experiment, and the data from the corner sections were discarded. The route and data collected during the rotation of the USV were not used for evaluating the performance of the proposed sensor model because these data sets could cause errors. Figure 9 shows the picture of experimental environment.

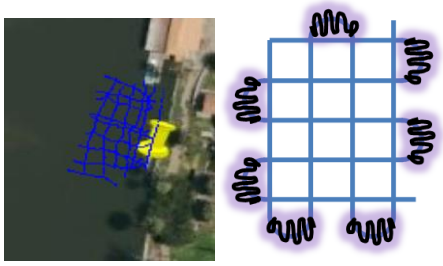

Fig.8. Top view of USV's moving route without the non-straight paths

Fig.9. Picture of experimental environment

C. Results

Table 3 lists 3D shapes of the underwater terrain before and after applying the proposed method using the data collected in the experiment. From the raw sonar data zoomed in, it is known that the ECHO park lake has been tilted slightly toward the center of the lake (left part of Fig. 8). In addition, wrong measurements indicating the lower of the terrain bottom are shown frequently (blue dots). An examination of the underwater terrain shapes at 0°, 30°, 50°, 70°, and 90° before filtering the data through the proposed underwater sonar sensor model shows indications of multiple points distributed uncertainly in the depth direction. These unnecessary points were due to inaccuracies in the sensor, and require filtering. The underwater terrain after applying the proposed sonar sensor model shows a significant reduction in these unnecessary points. Furthermore, the depth standard deviations were noticeably reduced after the application of the advanced sonar sensor model. The averages of depth standard deviation in the raw sonar data and the grid map result are 0.7115m and 0.464m respectively. Hence, the underwater terrain appears to be reducing the depth standard deviation by almost 35%. The coverages of underwater terrain are 231m^2 and 135m^2 respectively. The grid map built by the proposed sonar sensor model covered only 58.44% of the terrain of raw sonar data.

TABLE.3. Raw Data of Sonar Sensor and Grid Map Result after Applying the Proposed Sonar Sensor Model

View angle	Raw sonar data	Grid map result
90°	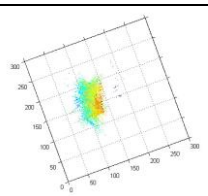	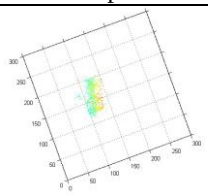
70°	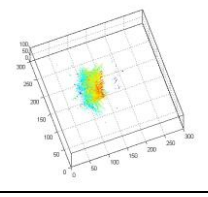	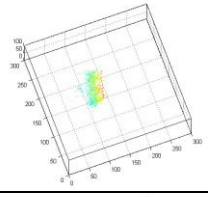
50°	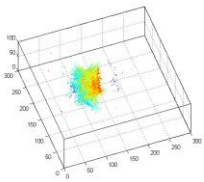	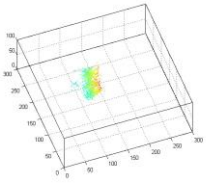
30°	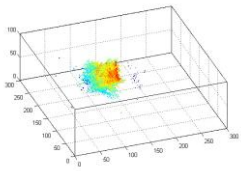	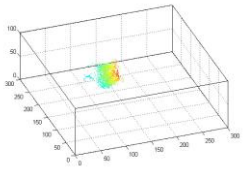
0°	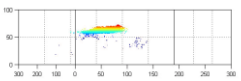	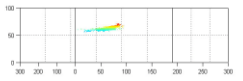
zoom in	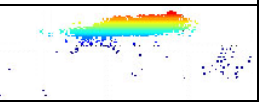	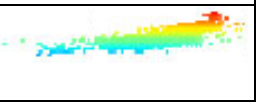

TABLE.4. Evaluation Results according to the depth standard deviation and coverage

	Raw sonar data	Grid map result
	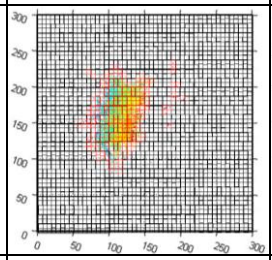	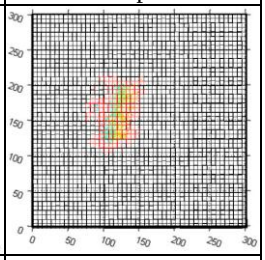
Depth standard deviation average	0.7115m	0.464m
Coverage	231m^2	135m^2

Conclusion

The advanced sonar sensor model capable of building an underwater terrain map based on the Bayes filter in the manner of the occupancy grid was presented in this paper. The proposed sonar sensor model basically considered the losses of received ultrasound intensity according to the underwater absorption and reflection on a terrain surface. The Bayes filter including the advanced sonar sensor model was applied to build the occupancy grid map. The previous section confirmed that the underwater terrain appeared to be more even after applying the proposed Bayes filter compared to before its application. Furthermore, a more accurate underwater topographic map was produced as a result of a significant reduction in the depth standard deviations. Therefore, it could be said that the proposed sensor model is suitable for creating underwater topographic maps. However, because a small number of correct data values were also filtered when filtering the unnecessary data, the coverage was so weak to represent a full terrain from the point cloud of sonar data. This part requires modification as the future work.

Acknowledgement

This work was supported by the research grant (2014-0643) of the Kongju National University in 2014.

References

[1] J.E. Manley, Unmanned surface vehicles, 15 years of development, Proc. of Oceans 2008, Quebec City, QC, 2008, 1-4.

[2] http://www.google.com/earth/

[3] http://www.koreaherald.com/view.php?ud=20140501000824

[4] The Navy Unmanned Undersea Vehicle(UUV) Master Plan, US Navy, 2004.

[5] Defense Robot Master Plan, Korea Agency for Defense Development, 2005.

[6] Report on Unmanned System for the Sea, Korea Agency for Defense Development, 2006.

[7] M. Jakuba and D. Yoerger, High-resolution multibeam sonar mapping with the Autonomous Benthic Explorer(ABE), Proc. the 13th Unmanned Untethered Submersible Technology Conference, Durham, NH, 2003.

[8] D. Langer and M. Hebert, Building Qualitative Elevation Maps From Side Scan Sonar Data For Autonomous Underwater Navigation, Proc. of the IEEE International Conference on Robotics and Automation, Sacramento, CA, 1991, 2478-2483.

[9] N. Fairfield, G.Kantor, and D. Wettergreen, Real-time SLAM with octree evidence grids for exploration in underwater tunnels, Journal of Field Robotics, 24(1-2), 2007, 3-21.

[10] S. B. Williams, P. Newman, J. Rosenblatt, G. Dissanayake, and H. Durrant-Whyte, Autonomous underwater navigation and control, Robotica, 19, 2001, 481-496.

[11] P. Newman, J. Leonard, and R. Rikoski, Towards constant-time slam on an autonomous underwater vehicle using synthetic aperture sonar, Proc. of 11th Int. Symp. On Robotics Research, Sienna, Italy, 2005, 409-420.

[12] I. T. Ruiz, S. Raucourt, Y. Petillot, and D. M. Lane, Concurrent Mapping and Localization Using Sidescan Sonar, IEEE Journal of Oceanic Engineering, 29(2), 2004, 442-456.

[13] Yun-Kyu Choi and Se-Jin Lee, Development of Advanced Sonar Sensor Model using Data Reliability and Map Evaluation Method for Grid Map Building, Journal of Mechanical Science and Technology, 29(2), 2015, 485-491.

[14] Jong-Hwan Lim and Chul-Ung Kang, Grid-Based Localization of a Mobile Robot Using Sonar Sensors, Journal of Mechanical Science and Technology, 16(3), 2002, 302-309.

[15] Se-Jin Lee, Dong-Woo Cho, and Jong-Hwan Lim, Effective Localization of Mobile Robots Using a Sonar Sensor Ring, International Journal of Robotics and Automation, 25(3), 2010, 186-194.

[16] http://www.nrl.navy.mil/content.php?P=03REVIEW212